



Floquet topological insulators with spin-orbit coupling

Adrian Pena  and Cristian Radu

National Institute of Materials Physics, Atomistilor 405A, 077125 Măgurele–Ilfov, Romania

 (Received 28 July 2023; revised 6 October 2023; accepted 26 January 2024; published 12 February 2024)

In a milestone paper [F. D. M. Haldane, *Phys. Rev. Lett.* **61**, 2015 (1988)], Haldane elaborated a model of graphene within the time-reversal symmetry breaking is achieved by next-nearest-neighbors imaginary counter-rotating hopping, hence conferring topological properties. In recent years, the time-reversal symmetry turned out to be broken also by light irradiation in so-called Floquet topological insulators (FTIs). On the other hand, Kane and Mele introduced a spin-orbit coupling (SOC) model [C. L. Kane *et al.*, *Phys. Rev. Lett.* **95**, 226801 (2005)] inspired by the Haldane's mechanism. In this paper, we present the topological properties of a FTI possessing SOC, using graphene as the playground. It was found that the interplay between sublattice subspace and the spin one triggers interesting topological phase transitions. Basically, in a FTI with SOC, two topological phases may be excited: charge quantum Hall effect (CQHE) and, respectively, spin quantum Hall effect (SQHE) phases. Also, it was demonstrated that the CQHE and SQHE coexistence is forbidden by the topology of the system. As well, it was identified a special driving regime of spin filter (SF), in which only one spin state is topological and, consequently, will be filtered in quantum transport.

DOI: [10.1103/PhysRevB.109.075121](https://doi.org/10.1103/PhysRevB.109.075121)

I. INTRODUCTION

Symmetries are the main aspect in the physics of topological insulators [1]. On the other hand, the dimensionality of the system also plays a high importance role. 2D topological insulators, so-called Chern insulators, are materials endowed with time-reversal symmetry and by breaking it, the topological phase transition is achieved [2]. In particular, a very interesting time reversal symmetry breaking mechanism is the circularly polarized light irradiation, and the systems in question are called Floquet topological insulators (FTIs) [3,4].

In recent years, the spin-orbit interaction was also included in the topological phases of matter studies and the findings were very promising for a future spintronics technology. The concept of spin-resolved topology was already studied in FTIs such as semiconductor quantum wells [5,6] and cold atoms trapped in optical lattices [7–9].

So far, graphene [10] has established itself as the emblematic material within the Chern insulators class. In a milestone paper [11], in 1988, Haldane introduced a model of time-reversal symmetry breaking in graphene via a next-nearest-neighbors imaginary counter-rotating hopping. Along recent years, it was observed that the mechanism proposed by Haldane is accomplished by light irradiation [12–19], hence inducing a Floquet topological phase. In an other valuable work [20], in 2005, Kane and Mele developed a model for spin-orbit coupling (SOC), which describes the topological properties of spin-resolved physics of graphene.

Starting from Haldane and Kane-Mele models [11,20], in this work, we investigate the topological properties of FTIs possessing an intrinsic SOC, as discussed also in Ref. [21] and in an extended Kane-Mele model containing disorder in Ref. [22]. We find that in a FTI with SOC, two topological phases may be excited, namely charge quantum Hall effect and, respectively, spin quantum Hall effect and their coexistence is forbidden by the intrinsic topology of the system.

The present work is organized as follows. In Sec. II, we present the model and discuss how the light interaction is introduced. In Sec. III, the main findings are discussed. Here, we elaborate a topological phase diagram based on Chern numbers and explain each phase in terms of energy band structure. Also, we interpret the topological phases in question in terms of quantum charge and spin transport. Finally, in Sec. IV, we summarize the main findings of our work.

II. THEORY

We analyze the interaction of a honeycomb lattice system (graphene) possessing an intrinsic SOC with light. The light is introduced in our problem via the following time-dependent vector potential (plane wave approximation):

$$\mathbf{A}(t) = A_0[\cos(\omega t)\hat{\mathbf{x}} + \Lambda \sin(\omega t)\hat{\mathbf{y}}]. \quad (1)$$

In Eq. (1), A_0 is a real constant amplitude representing the magnitude of the vector potential, ω is the frequency, $\Lambda = \pm 1$ is the helicity quantum number, and $\hat{\mathbf{x}}(\hat{\mathbf{y}})$ is the unit vector along the $x(y)$ axis. We consider the graphene sheet lying in the horizontal plane, while the light is propagating at normal incidence. Schematically, the system in question is described in Fig. 1(a). The honeycomb lattice of graphene is depicted in Fig. 1(b), where the unit cell is represented by the gray shaded area and contains two atoms indexed by A (blue) and, respectively, B (red). The distance between two nearest-neighbors A and B is denoted by a . In what follows, we employ the tight-binding approach, using the second quantization formalism, where the operator $a_i^\dagger(b_i^\dagger)$ creates a particle of type $A(B)$ at the atomic site indexed by i and, respectively, $a_j(b_j)$ annihilates a particle of type $A(B)$ at the atomic site j . In the

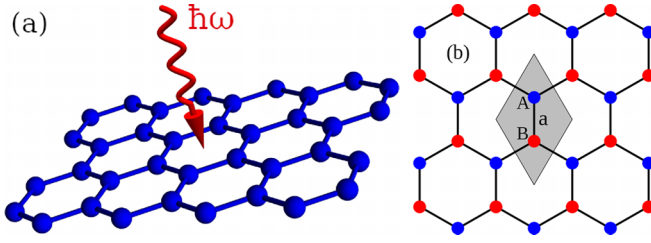


FIG. 1. Schematic description of the studied system. (a) The graphene is placed on the horizontal plane, while the light ($\hbar\omega$) is propagating on the perpendicular direction. (b) The honeycomb lattice. The unit cell, represented by the gray shaded area, contains two atoms indexed by A (blue) and, respectively, B (red).

framework discussed above, the time-dependent Hamiltonian of the system reads with the following equations:

$$H(t) = \sum_{\sigma=\pm 1} (H_0^\sigma(t) + H_{SO}^\sigma(t)), \quad (2)$$

$$H_0^\sigma(t) = -\gamma \sum_{\langle A_i, B_j \rangle} \text{Exp}[i\theta_{i,j}(t)] a_i^\dagger b_j + \text{H.c.}, \quad (3)$$

$$H_{SO}^\sigma(t) = \frac{i}{2} \lambda_{SO} \sigma \sum_{\langle\langle A_i, A_j \rangle\rangle} v_{ij} \text{Exp}[i\theta_{ij}(t)] a_i^\dagger a_j + a \leftrightarrow b + \text{H.c.} \quad (4)$$

The first term in the expression of the total Hamiltonian (2), defined in Eq. (3), expresses the interaction of the honeycomb lattice system with light in the absence of SOC, where $\gamma = 2.8$ eV represents the hopping amplitude between nearest-neighbors $\langle A_i, B_j \rangle$. The second term, defined in Eq. (4), introduces in our problem the SOC, as discussed by Kane and Mele in Ref. [20], where λ_{SO} gives the coupling strength, $\sigma = \pm 1$ is the spin quantum number, and $v_{ij} = \pm 1$, depending on the next-nearest-neighbors hopping direction (counterclockwise and, respectively, clockwise). Note that in the actual model, besides the nearest-neighbors real valued hopping within Eq. (3), we deal also with an imaginary next-nearest-neighbors hopping $\langle\langle A_i, B_j \rangle\rangle$, realizing a Haldane model, proposed in Ref. [11]. Explicitly, the interaction with light is introduced via Peierls phases, defined by the following path integral:

$$\theta_{ij}(t) = \frac{e}{h} \int_{i \rightarrow j} \mathbf{A}(t) \cdot d\mathbf{l}, \quad (5)$$

where e is the elementary charge constant, h is the Plank constant, $\mathbf{A}(t)$ is the vector potential defined in Eq. (1), and $d\mathbf{l}$ parametrizes the path between i and j atomic sites.

Since the time periodicity is an intrinsic property of the light and implicitly of the Hamiltonian (2), in what follows we utilize the Floquet formalism [23–27]. Within this approach, the energy scales are crucial in formulating the appropriate Hamiltonian. For a photon energy $\hbar\omega \gg 6\gamma$, where 6γ represents the band width of the energy spectrum of graphene, the system is described in good agreement by the following high frequency Hamiltonian [19] (see the Supplemental Material

[28]):

$$H_{\text{HF}} = H_0 + \frac{1}{\hbar\omega} [H_{-1}, H_1], \quad (6)$$

$$H_n = \frac{1}{T} \int_0^T dt e^{in\omega t} H(t). \quad (7)$$

Taking into account the integral (7), within each H_n term, the Peierls substitution will transform as

$$\text{Exp}[i\theta(t)] \rightarrow i^n J_n \left(\frac{eaA_0}{h} \right) e^{\Lambda i n \varphi}, \quad \text{for Eq. (3)}, \quad (8)$$

$$\text{Exp}[i\theta(t)] \rightarrow i^n J_n \left(\frac{ea\sqrt{3}A_0}{h} \right) e^{\Lambda i n \varphi}, \quad \text{for Eq. (4)}. \quad (9)$$

Here, $J_n(x)$ represents the first kind Bessel function, e the elementary charge constant, h the Planck constant, and φ the direction between the adjacent atoms between the hopping takes place. See the Supplemental Material [28] for proof.

III. NUMERICAL RESULTS AND DISCUSSION

The Fourier space of graphene has a honeycomb structure, as its real space, where each hexagon corner represents a high symmetry point, called a Dirac point or K point. In these special points in the Brillouin zone, the energy bands close, forming so-called Dirac cones where the energy disperses linearly. However, when the graphene is driven by light, the Dirac cones vanish and, around each K point, an energy gap arises. If the system is confined on one direction (ribbon), within the energy gaps two symmetrically crossed chiral bands emerge. These two bands have a striking property. First, each of them hosts a well defined A or B state which also has a well defined momentum direction. Second, the states we are discussing here are strongly and separately confined at the edges of the system, so-called chiral edge states. Therefore, in the Floquet topological phase, in graphene emerge two conduction channels localized at the edges and to each channel a well defined A or B state participates. In this way, the circularly polarized light driving triggers an anomalous quantum Hall effect (QHE). This phenomenon was first discussed in Refs. [12,13,15,17,18]. For an in-depth analysis we refer the reader to Ref. [29].

In what follows we express all the (quasi)energies in terms of hopping amplitude γ and the magnitude of the light vector potential in terms of $h/(ea)$.

When the SOC is present, automatically a supplementary degree of freedom is introduced, and that is the spin quantum number $\sigma = \pm 1$. As discussed by Kane and Mele in Ref. [20], a SOC term present in the graphene Hamiltonian opens a gap in the energy spectrum, where two spin-degenerate symmetrically crossed bands appear. However, these two bands are not chiral, therefore the charge QHE (CQHE) condition is not fulfilled. Instead, the spin QHE (SQHE) phase is achieved.

For a comprehensive investigation, we start by analyzing a honeycomb lattice with SOC under light driving, in an infinite configuration. In order to characterize the band structure of the system, we perform the Fourier transform of real space Hamiltonian (6). In Figs. 2(a) and 2(b), we present the quasienergy dispersion on the $K'-\Gamma-K$ direction in the Brillouin zone, for $A_0 = 0.6$, $\Lambda = 1$, and $\hbar\omega = 10$. The SOC

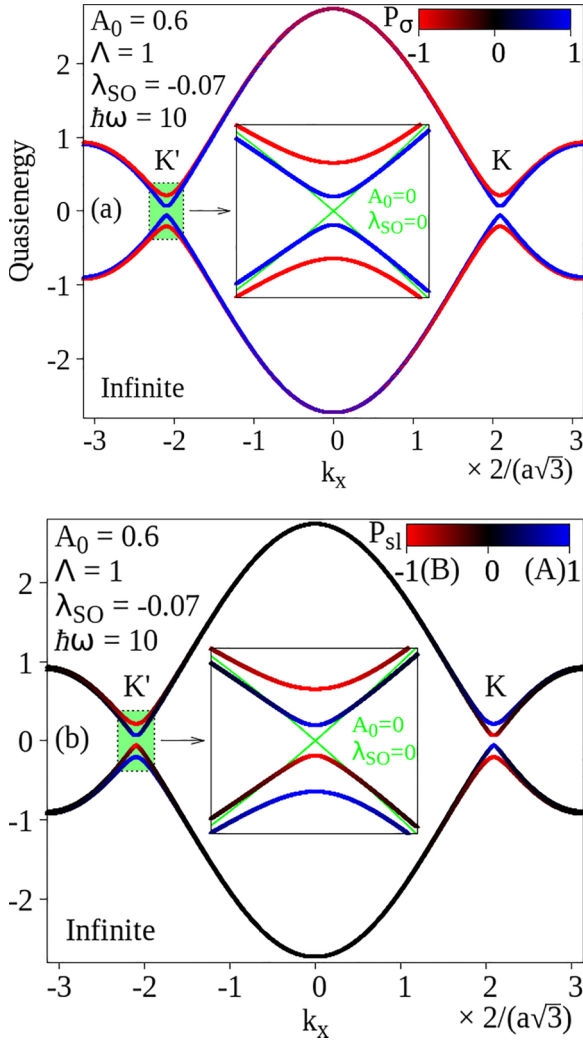


FIG. 2. Band structure of graphene with SOC under light irradiation, on direction $K'\text{-}\Gamma\text{-}K$: (a) for spin and (b) for sublattice polarization. The insets present a zoomed view around K' . The green energy bands within the insets are plotted for a graphene in the absence of SOC and light irradiation.

strength is $\lambda_{\text{SO}} = -0.07$, a value of approximately 200 meV, already realized experimentally, see Ref. [30]. Now, in order to characterize the degeneracy and its lifting, we introduce the sublattice polarization function (see Appendix for derivation):

$$P_{\text{sl}}(\mathbf{k}) = \frac{|\langle A_n(\mathbf{k})|A_n(\mathbf{k})\rangle| - |\langle B_n(\mathbf{k})|B_n(\mathbf{k})\rangle|}{|\langle A_n(\mathbf{k})|A_n(\mathbf{k})\rangle| + |\langle B_n(\mathbf{k})|B_n(\mathbf{k})\rangle|}, \quad (10)$$

where $n = 1, 2$ represents the band index. The function (10) takes values in the interval $[-1, 1]$ and have the following interpretation. For instance, if $P_{\text{sl}} = 1$, an energy band at a given k_x participates exclusively in A state. For $P_{\text{sl}} = -1$, there participates exclusively a B state. For any other value, the participation is from both A and B states, each of them with a specific weight. By analogy, we also introduce the spin polarization function denoted by P_{σ} with $\sigma = \pm 1$, having the same interpretation as P_{sl} .

As revealed in panel (a), around each Dirac point, an energy gap arises, which is due to the light interaction and SOC, as discussed above. Interestingly, the light irradiation

lifts the spin degeneracy and in the vicinity of Dirac points the bands are completely spin polarized. In the inset is presented a zoomed view around K' , where the dispersion in the absence of light and SOC is plotted with green. Here, we obviously observe the intersection of the two green bands, forming a Dirac cone where the energy disperses linearly. The most important effect we observe here is that the gaps have different magnitudes for each spin state. In our example, the gap for $\sigma = +1$ is lower than for $\sigma = -1$. This behavior leads us to the following prediction. If the light drives the system differently, depending on the spin state, the corresponding bands will close and open one after the other. On the other hand, since the topological phase transition is accompanied mandatorily by a band closing, the topological phase diagram will be automatically spin resolved. Note that the spin polarization is the same for both K' and K points. Going further, we investigate the interaction also in sublattice polarization terms, for the same parameters as in panel (a). As depicted in panel (b), around the two Dirac points, the bands are also polarized in A and B states. If we move from one Dirac point to the other, unlike in the case of spin-polarization analysis, we observe that the sublattice polarization is reversed. Consequently, both the large and small gaps are bordered by bands containing both A and B states. Recall that this situation is not the same in the case of spin states.

Since we are dealing with a bipartite spin subspace, we can define a spin Chern number C_{σ} [31–33] associated to each $\sigma = \pm 1$ spin state for the lower spin bands (below zero quasienergy level). The spin Chern number characterizes the topology of the system with respect to a well defined spin state and, hence, will govern the SQHE phase. As well, since intrinsic SOC is spin-conserving, we also define a spin-summed Chern number:

$$C = C_{-1} + C_1. \quad (11)$$

The topological invariant defined above globally characterizes the system assuming that the Fermi level always lies within the quasienergy gap and will govern the CQHE phase.

Panel (a) of Fig. 3 represents the topological phase diagram, computed using the Fukui-Hatsugai-Suzuki method [34]. The top plot shows the spin Chern number C_{σ} , while the bottom one is for spin-summed Chern number C . Analyzing the topological transitions, we distinguish different regimes of light driving. Whenever $C_{-1} = -C_{+1}$, the system lies in a SQHE phase (yellow regions), and in transport terms only spin states are transversely transmitted with opposite direction. Since in this phase $C = 0$, the system will not transport any charge. On the other hand, when $C_{-1} = C_{+1} = 1$ and $C = 2$, the QSHE is quenched and the system is in a CQHE phase (gray regions), then only charge will be transported. Moreover, we expect a Hall resistance $R_H = \frac{1}{2} e/h^2$. Interestingly, the values $C = -2$ are forbidden. This phenomenon is related to the helicity of the driving light. Examining Eqs. (8) and (9), we observe that the substitution $\Lambda \rightarrow -\Lambda$ is equivalent to changing $\varphi \rightarrow -\varphi$ or $y \rightarrow -y$. Since this transformation rotates the system about the x axis, the direction of the edge states momentum will be inverted, therefore also C changes its sign. In this way, if $\Lambda = -1$ the conduction channels localized at the edges of the lattice will also revert their direction, hence the charge will be transported implicitly on the opposite

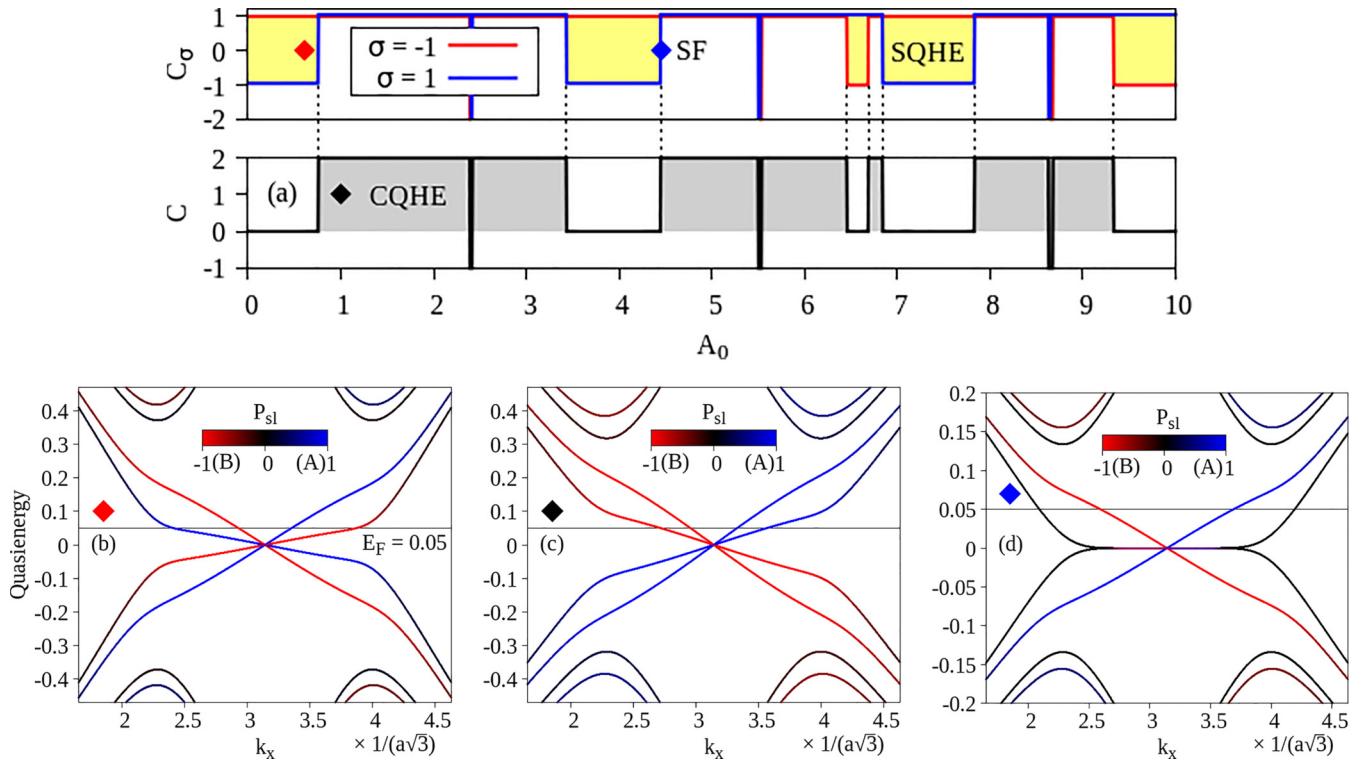


FIG. 3. Topological phase diagram vs A_0 (upper panel) and quasienergy dispersion for a ribbon with zig-zag termination and ten atoms in the unit cell (lower panels): (b) SQHE [yellow regions within (a)], (c) CQHE (black regions), and (d) SF driving regime (blue marker).

direction than before. This effect will generate a Hall resistance $R_H = -\frac{1}{2} e/h^2$. Concerning the spin states, the same behavior is valid. Having in mind the discussion above, when changing the light helicity state, also the next-nearest-neighbors hopping directions are inverted [$v_{ij} \rightarrow -v_{ij}$ in Eq. (4)] and this is the same as changing the spin state ($\sigma \rightarrow -\sigma$). Resuming, the change $\Lambda \rightarrow -\Lambda$ determines $C \rightarrow -C$ and $C_\sigma \rightarrow -C_{-\sigma}$, and this is one of the most important phenomena which happens in a FTI with SOC (see Fig. S3(a) in the Supplemental Material [28]). Besides SQHE and CQHE phases, we can identify a special regime of spin filtering (SF). This occurs when one spin state gap remains open, while the other closes. Namely, this effect takes place every time when one of C_σ changes its sign, see for instance blue marker where C_{-1} becomes 1 from -1 .

In terms of quasienergy dispersion and band chirality, the topological phases examined above are described in Fig. 3, panels (b) for SQHE [red marker within panel (a)], (c) for CQHE (black marker), and (d) for SF driving regime, respectively. Analyzing the quasienergy dispersion, we observe three different configurations. In what follows we assume a Fermi level (FL) $E_F = 0.05$ residing in the topological gap. First, in the SQHE phase the FL is crossing four chiral bands having alternating chiralities. In this configuration, at the edges of the system will arise two A and B states. The A type states will be localized on one edge and, respectively, B type states, at the other edge. However, as the slope of the chiral bands indicates, at each edge will arise two conduction channels with opposite directions. Hence, the charge Hall transport should vanish. Second, in the CQHE phase, the FL also crosses four chiral bands, but this time, A type states will have a positive

momentum direction and, respectively, B states will have a negative one. As a result, at one edge will arise two conduction channels with the same direction and at the other edge, two conduction channels with the other direction. In this way, the system transports charge in the transversal direction, in a Hall device configuration. Finally, in the SF regime, the FL crosses only two chiral bands, populated with $\sigma = -1$ spin state. The other nonchiral bands, corresponding to $\sigma = +1$ spin state, are exactly the same as when the system was not driven by light and the SOC was absent. In other words, the $\sigma = +1$ state shows simply a pristine zig-zag terminated graphene ribbon dispersion. These two nonchiral bands accommodate nonlocalized states. This last interpretation is best summarized in the Supplemental Material [28], where we show the local density of states (LDOS) for each $A, B, \sigma = \pm 1$ state. In the case of $\Lambda = -1$, the bands chirality within panels (b), (c), and (d) is reversed (see panels (b), (c) and (d) of Fig. S3 in the Supplemental Material [28]).

In Fig. 4, we present transport results using Landauer-Büttiker formalism [35,36] (see the Supplemental Material [28] for details). The spin-resolved Hall resistance is denoted by $R_{H\sigma}$, while R_H expresses the charge transport. In what follows, the constant h/e^2 will be dropped. In panel (a), the SQHE (top plot) and CQHE (bottom plot) are highlighted vs A_0 . The Hall resistance specific plateaus are in perfect agreement with the topological phase transitions explored in terms of Chern numbers and quasienergy dispersion within the topological gaps opened by light driving and SOC. Moreover, in panel (b), we investigated the transport effects with respect to FL in the SF regime [see blue marker in Fig. 3(d)]. In the SF regime, the $\sigma = -1$ state gap is still open, while the

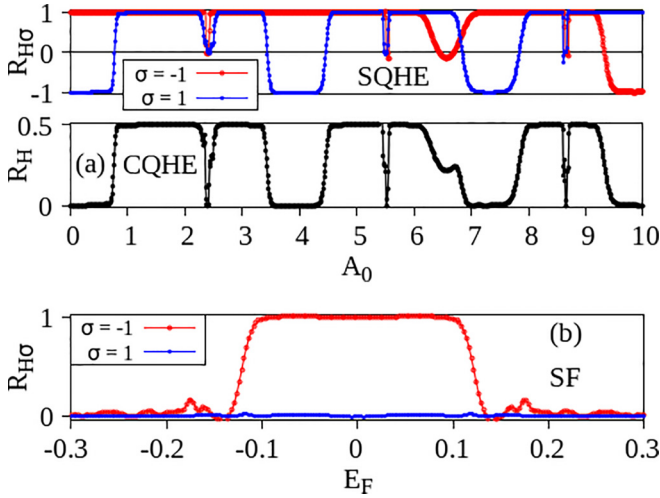


FIG. 4. Quantum Hall transport diagram. (a) SQHE (top panel) and CQHE (bottom panel) vs A_0 . $R_{H\sigma}$ (R_H) plateaus are in perfect agreement with the topological phase diagram [Fig. 3(a)]. (b) $R_{H\sigma}$ in SF driving regime vs E_F . The state $\sigma = -1$ is filtered.

corresponding $\sigma = +1$ closes, therefore only $\sigma = -1$ states will be topological. In the configuration discussed here, the spin Hall transport will be achieved only for $\sigma = -1$, as long as the FL resides in the topological gap. As a result, in the transport diagram R_{H-1} will show a $+1$ plateau, while R_{H+1} vanishes. That is to say the $\sigma = -1$ spin will be filtered in the transversal direction. Finally, when $\Lambda = -1$, as discussed, the chirality is reversed and, hence, the Hall plateaus will change their sign and also spin state. See the Supplemental Material [28] for results.

SF represents a transitional regime and thus it may be seen as a critical property. The SF is realized whenever the spin Chern number C_σ changes its sign, namely at a topological phase transition. On the other hand, each phase transition is determined by an energy gap closing. Here, the main important property is represented by the spin conservation, thus the entire system may be understood as two noninteracting subsystems (one for $\sigma = -1$ and one for $\sigma = +1$). Having in mind this property, the spin-resolved topological phase transitions realize independently. In the Floquet model proposed in our manuscript, the spin-resolved energy gap G_σ is governed by the following functions:

$$G_{\sigma=+1} = \frac{3\sqrt{3}}{5} |\sqrt{3}J_1^2(A_0) - 5\lambda_{\text{SO}}J_0(\sqrt{3}A_0)|, \quad (12)$$

$$G_{\sigma=-1} = \frac{3\sqrt{3}}{5} |\sqrt{3}J_1^2(A_0) + 5\lambda_{\text{SO}}J_0(\sqrt{3}A_0)|. \quad (13)$$

Consequently, whenever A_0 takes a value for which $G_{\sigma=\pm 1} = 0$, the TRS is not broken, thus the subsystem behaves simply as a graphene with renormalized hopping parameters. In this case, only one spin state (subsystem) lies in a topological phase and, by consequence, will be filtered in a Hall transport experiment.

Finally, we suggest a feasible experimental method to probe the theory discussed in this manuscript. First, for the fabrication of the graphene sample, we invoke Ref. [30], which demonstrated that a layer of Pb intercalated between a

monolayer graphene sheet deposited on Pt(111) enhances the SOC up to a value of 200 meV. Otherwise, another technique for SOC increasing consists of a controlled hydrogenation, as shown in Refs. [37,38]. Second, the graphene based Hall transport device may be set up by attaching a number of electrodes using the method presented in Ref. [39]. Third, the measurements under circularly polarized light irradiation [13,40] must be performed in the presence of a microwave excitation as already realized in Refs. [41–43].

IV. CONCLUSION

To summarize, we have explored the topological properties of a FTI with an intrinsic SOC. The interplay between the sublattice subspace and the spin one turned out to be the trigger of topological phase transitions. With respect to A_0 , which in turn dictates the driving light intensity, we have identified two phases, namely SQHE and CQHE, whose coexistence is forbidden by the topology of the system. Moreover, we have also distinguished a special driving regime of SF, in which only one spin state is topological and, hence, will be filtered in quantum transport. All the topological properties described in the present paper were explained correlating the abstract method of Chern numbers with quasienergy spectral properties. Finally, we have discussed the transport phenomena from the perspective of topological features presented in the first part of this work.

ACKNOWLEDGMENT

This work was supported by grants of the Ministry of Research, Innovation and Digitization through the Core Program PC2-PN23080202 within PNCDI 2022-2027.

APPENDIX A: SUBLATTICE POLARIZATION FUNCTION

In this Appendix we present a rigorous definition and interpretation for Eq. (10).

In infinite configuration, where the unit cell contains two atoms (A and B), the system is described by the following two-component uniparticle wave function:

$$|\psi_n(\mathbf{k})\rangle = \alpha_n(\mathbf{k})|a\rangle + \beta_n(\mathbf{k})|b\rangle, \quad (A1)$$

where the basis kets $|a\rangle$ and $|b\rangle$ satisfy

$$\langle a|a\rangle = \langle b|b\rangle = 1 \quad \text{and} \quad \langle b|a\rangle = 0. \quad (A2)$$

In Eq. (A1), $n = 1, 2$ represents the band index. The complex coefficients $\alpha_n(\mathbf{k})$ and $\beta_n(\mathbf{k})$ express the contribution of each A and B state. The normalization of the wavefunction (A1) in the sublattice space implies

$$|\alpha_n(\mathbf{k})|^2 + |\beta_n(\mathbf{k})|^2 = 1. \quad (A3)$$

Now consider the following projectors on A and B states, respectively:

$$P_A = |a\rangle\langle a| \quad \text{and} \quad P_B = |b\rangle\langle b|. \quad (A4)$$

Using (A4), we define the following states:

$$|A_n(\mathbf{k})\rangle = P_A|\psi_n(\mathbf{k})\rangle \quad \text{and} \quad |B_n(\mathbf{k})\rangle = P_B|\psi_n(\mathbf{k})\rangle. \quad (A5)$$

In Eq. (10), the numerator reads

$$|\langle A_n(\mathbf{k})|A_n(\mathbf{k})\rangle| - |\langle B_n(\mathbf{k})|B_n(\mathbf{k})\rangle| = |\alpha_n(\mathbf{k})|^2 - |\beta_n(\mathbf{k})|^2. \quad (\text{A6})$$

Hence, taking into account Eqs. (A3) and (A6), the function defined by Eq. (10) (sublattice polarization, P_{sl}) expresses the difference between A and B states contribution at any given

\mathbf{k} . Say, for instance, at a given \mathbf{k}_1 in the n th band, $P_{sl} = 1$, hence $|\alpha_n(\mathbf{k}_1)|^2 = 1$ and the wavefunction (A1) entirely represents state A . In other words, at \mathbf{k}_1 point, the band n is fully polarized in A states. On the other hand, if in \mathbf{k}_2 , $P_{sl} = -1$, the respective band is fully polarized in B states. Going further, if in \mathbf{k}_3 , $P_{sl} = 0$, the band is fully nonpolarized.

-
- [1] J. E. Moore, *Nature (London)* **464**, 194 (2010).
 [2] M. Z. Hasan and C. L. Kane, *Rev. Mod. Phys.* **82**, 3045 (2010).
 [3] M. S. Rudner and N. H. Lindner, *Nat. Rev. Phys.* **2**, 229 (2020).
 [4] F. Harper, R. Roy, M. S. Rudner, and S. L. Sondhi, *Annu. Rev. Condens. Matter Phys.* **11**, 345 (2020).
 [5] N. H. Lindner, G. Refael, and V. Galitski, *Nat. Phys.* **7**, 490 (2011).
 [6] F. Qin, C. H. Lee, and R. Chen, *Phys. Rev. B* **106**, 235405 (2022).
 [7] Z. Yan, B. Li, X. Yang, and S. Wan, *Sci. Rep.* **5**, 16197 (2015).
 [8] T. Schuster, F. Flicker, M. Li, S. Kotochigova, J. E. Moore, J. Ye, and N. Y. Yao, *Phys. Rev. Lett.* **127**, 015301 (2021).
 [9] T. Schuster, F. Flicker, M. Li, S. Kotochigova, J. E. Moore, J. Ye, and N. Y. Yao, *Phys. Rev. A* **103**, 063322 (2021).
 [10] A. H. Castro Neto, F. Guinea, N. M. R. Peres, K. S. Novoselov, and A. K. Geim, *Rev. Mod. Phys.* **81**, 109 (2009).
 [11] F. D. M. Haldane, *Phys. Rev. Lett.* **61**, 2015 (1988).
 [12] T. Oka and H. Aoki, *Phys. Rev. B* **79**, 081406(R) (2009).
 [13] J. Karch, P. Olbrich, M. Schmalzbauer, C. Zoth, C. Brinsteiner, M. Fehrenbacher, U. Wurstbauer, M. M. Glazov, S. A. Tarasenko, E. L. Ivchenko *et al.*, *Phys. Rev. Lett.* **105**, 227402 (2010).
 [14] T. Kitagawa, E. Berg, M. Rudner, and E. Demler, *Phys. Rev. B* **82**, 235114 (2010).
 [15] J. Karch, C. Drexler, P. Olbrich, M. Fehrenbacher, M. Hirmer, M. M. Glazov, S. A. Tarasenko, E. L. Ivchenko, B. Birkner, J. Eroms *et al.*, *Phys. Rev. Lett.* **107**, 276601 (2011).
 [16] P. Delplace, Á. Gómez-León, and G. Platero, *Phys. Rev. B* **88**, 245422 (2013).
 [17] A. Kundu, H. A. Fertig, and B. Seradjeh, *Phys. Rev. Lett.* **113**, 236803 (2014).
 [18] P. M. Perez-Piskunow, G. Usaj, C. A. Balseiro, and L. E. F. Foa Torres, *Phys. Rev. B* **89**, 121401(R) (2014).
 [19] T. Mikami, S. Kitamura, K. Yasuda, N. Tsuji, T. Oka, and H. Aoki, *Phys. Rev. B* **93**, 144307 (2016).
 [20] C. L. Kane and E. J. Mele, *Phys. Rev. Lett.* **95**, 226801 (2005).
 [21] M. Berdakin, E. A. Rodríguez-Mena, and L. E. F. Foa Torres, *Nano Lett.* **21**, 3177 (2021).
 [22] L. Du, P. D. Schnase, A. D. Barr, A. R. Barr, and G. A. Fiete, *Phys. Rev. B* **98**, 054203 (2018).
 [23] J. H. Shirley, *Phys. Rev.* **138**, B979 (1965).
 [24] H. Li, B. Shapiro, and T. Kottos, *Phys. Rev. B* **98**, 121101(R) (2018).
 [25] C. Wurl and H. Fehske, *Phys. Rev. A* **98**, 063812 (2018).
 [26] V. Junk, P. Reck, C. Gorini, and K. Richter, *Phys. Rev. B* **101**, 134302 (2020).
 [27] U. De Giovannini and H. Hübener, *J. Phys. Mater.* **3**, 012001 (2020).
 [28] See Supplemental Material at <http://link.aps.org/supplemental/10.1103/PhysRevB.109.075121> for complete mathematical derivations and additional numerical results.
 [29] A. Pena, *Results Phys.* **46**, 106257 (2023).
 [30] I. I. Klimovskikh, M. M. Otrokov, V. Y. Voroshnin, D. Sostina, L. Petaccia, G. Di Santo, S. Thakur, E. V. Chulkov, and A. M. Shikin, *ACS Nano*. **11**, 368 (2017).
 [31] D. N. Sheng, Z. Y. Weng, L. Sheng, and F. D. M. Haldane, *Phys. Rev. Lett.* **97**, 036808 (2006).
 [32] E. Prodan, *Phys. Rev. B* **80**, 125327 (2009).
 [33] Y. Yang, Z. Xu, L. Sheng, B. Wang, D. Y. Xing, and D. N. Sheng, *Phys. Rev. Lett.* **107**, 066602 (2011).
 [34] T. Fukui, Y. Hatsugai, and H. Suzuki, *J. Phys. Soc. Jpn.* **74**, 1674 (2005).
 [35] B. Ostahie, M. Nița, and A. Aldea, *Phys. Rev. B* **94**, 195431 (2016).
 [36] S. Datta, *Electronic Transport in Mesoscopic Systems* (Cambridge University Press, Cambridge, 1995).
 [37] M. Gmitra, D. Kochan, and J. Fabian, *Phys. Rev. Lett.* **110**, 246602 (2013).
 [38] J. Balakrishnan, G. K. W. Koon, M. Jaiswal, A. H. Castro Neto, and B. Özyilmaz, *Nat. Phys.* **9**, 284 (2013).
 [39] Z. Wang, D.-K. Ki, H. Chen, H. Berger, A. H. MacDonald, and A. F. Morpurgo, *Nat. Commun.* **6**, 8339 (2015).
 [40] J. W. McIver, B. Schulte, F.-U. Stein, T. Matsuyama, G. Jotzu, G. Meier, and A. Cavalleri, *Nat. Phys.* **16**, 38 (2020).
 [41] R. G. Mani, J. Hankinson, C. Berger, and W. A. de Heer, *Nat. Commun.* **3**, 996 (2012).
 [42] T. J. Lyon, J. Sichau, A. Dorn, A. Centeno, A. Pesquera, A. Zurutuza, and R. H. Blick, *Phys. Rev. Lett.* **119**, 066802 (2017).
 [43] J. Sichau, M. Prada, T. Anlauf, T. J. Lyon, B. Bosnjak, L. Tiemann, and R. H. Blick, *Phys. Rev. Lett.* **122**, 046403 (2019).